Exp Fluids (2010) 49:461–470
DOI 10.1007/s00348-009-0811-6

RESEARCH ARTICLE

Wall roughness effects in laminar flows: an often ignored though significant issue

D. Gloss · H. Herwig

Received: 20 January 2009 / Revised: 20 December 2009 / Accepted: 28 December 2009 / Published online: 13 January 2010

Abstract The effect of wall roughness, which is strong in turbulent flows often, is neglected in laminar flows, though without justification. With an experimental set-up which allows for changes in the relative roughness of a channel without requiring manipulation of the rough channel surface, it can be shown that there is a non-negligible influence of wall roughness even for laminar flows. Based on the consideration of entropy production in these flows, an increased dissipation rate in the vicinity of the roughness elements is identified as the physical mechanism that leads to an increased total head loss when the walls are no longer smooth.

1 Introduction

With the increase in micro fluidic and chip cooling in the last two decades, laminar flows through pipes and channels have become more important. Often in these devices, Reynolds numbers are well below the critical Reynolds number for transition to turbulence and thus laminar flows are the normal case.

As far as the influence of wall roughness is concerned until today, there still is the popular believe that "... for small Reynolds numbers there is no influence of wall roughness on the flow resistance" (translated from Nikuradse 1933). Even in most recent textbooks, like Munson et al. (2005), one can find statements like "For laminar flow, $f = 64/Re$, which is independent of relative roughness".

In almost all textbooks, the Moody chart appears, which displays the pipe friction factor as a function of the Reynolds number and the relative roughness with one line for the laminar case, i.e. without influence of wall roughness (see, for example, Schlichting and Gersten 2006; White 2008; Zierep 2008).

There is, however, a special situation for micro flow devices. Due to the manufacturing processes used in micro fabrication, walls are never perfectly smooth but often have some relative roughness. In these cases, people are aware of the influence wall roughness may have and special studies take it into account, as in Wu and Little (1983), Hu et al. (2003), Kleinstreuer and Koo (2004), Hao et al. (2006), Rawool et al. (2006), Brackbill and Kandlikar (2007), and Lilly et al. (2007).

The influence of wall roughness in laminar flows, however, is by no means restricted to microflows. Based on dimensional arguments (see Herwig 2002) it becomes evident that this influence likewise appears in macro-sized devices. It is only the relative roughness (roughness height compared to a characteristic length of the device) that counts. This has been taken into account in several previous studies already, like in Kandlikar (2005), Croce and D'Agaro (2005), and Ji et al. (2005).

In the present study a systematic approach to surface roughness impact on laminar flows is realized in an experimental set-up that (for reasons described later) has dimensions which often are classified as micro-sized. Micro flow investigations, however, are not the focus of our study. Laminar flows in general are investigated, and the results are gained that hold in all dimensions as long as the flow is a continuum flow of a Newtonian fluid subject to non-slip boundary conditions.

D. Gloss · H. Herwig (✉)
Hamburg University of Technology, Hamburg, Germany
e-mail: h.herwig@tuhh.de

D. Gloss
e-mail: daniel.gloss@tuhh.de

In our test facility, we systematically show that the influence of surface roughness cannot be neglected in laminar flows. We do this in a special geometry and for different kinds of wall roughness. Afterwards, we generalize our results by introducing a theoretical dissipation model which is validated by our experimental results and which from now on can be used as an alternative to the experimental determination of the roughness impact. Thus, the influence of wall roughness for a certain geometry can be determined either experimentally or by applying the (validated) numerical dissipation model.

2 The experimental set-up

The general requirements with respect to the experimental facility for roughness impact investigations are the following. The experimental set-up should:

(a) have freely accessible inner surfaces so that a particular surface roughness can be applied with high precision,
(b) allow for an increase of the roughness parameter $K = k/H$ without changing the surface structure, i.e. without changing the roughness elements on the wall, for example, with $0 < K < 0.1$,
(c) be free of entrance effects in the measurement range (sometime called *minor losses*). This can be assured with a downstream flow field length of at least 100 times the wall distance H.
(d) have a Reynolds number range of the order of $Re \approx 1$ to $Re \approx 1{,}000$

2.1 Basic geometry of the set-up

Figure 1 shows a sketch of an experimental set-up that meets the above requirements (a–d). The crucial idea is not to use rigid channels that are somehow manufactured within a carrier material. Instead, our channels appear between two surfaces that are brought close together with a distance that may be adjusted from case to case. Thus, we have channels with a fixed surface quality (roughness) but variable wall spacing (channel height).

In our set-up according to Fig. 1, the channel emerges between two symmetrical disks. The lower one carries the flow inlet at its centre and the pressure gauges. The upper disk holds a silicon wafer. To provide roughness elements, this wafer's surface can be manipulated using an etching technique. Wafers with different surface structures thus realize channels with different wall roughness. In order to change the *roughness type* of the channel only the wafer is changed. In order to change the *relative roughness* of the channel, only the channel heigt (wall distance) is adjusted. Details of the structuring technique are discussed in Sect. 2.2.

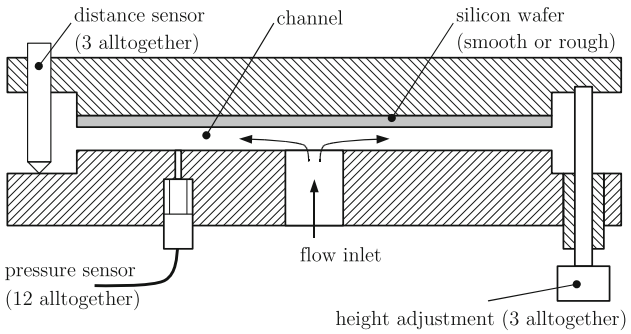

Fig. 1 Conceptual view of the experimental set-up, the silicon-wafer can either have a smooth or a rough surface

With the structuring of the wafer surfaces, a fixed roughness height k is produced. The roughness number $K = k/H$, as explained before, can be changed continuously by adjusting the gap between the disks and hence by changing H without manipulating the (rough) surface.

Various aspects of the experimental set-up are:

- channel length: 40 mm
- channel height: 20 μm $\leq H \leq$ 400 μm (continuously adjustable)
- measurable pressure drop: 50 Pa $\leq \Delta p \leq 10^4$ Pa
- medium: air or helium
- silicon wafer: processed (rough) or polished (smooth)

The gauge pressure can be measured at 12 different radial locations along the channel. The channel height is measured with three different distance sensors opposite to the three height adjustment devices.

Determination of the wall distance H is crucial to the results, however. As a definition for the wall location when walls are rough we prefer that H for an equivalent smooth channel, for which the real and the equivalent channel have the same fluid-filled volume, see Herwig et al. (2008a) for a discussion of various alternatives.

For a wafer with a regular and rectangular roughness geometry, for example, this means that the equivalent smooth wall is located exactly at $k/2$. Figure 2 shows a sketch of such a rough channel with size H and a roughness height k. A detailed description of the surface structuring technique to produce this geometry will be presented in the next section.

Although the size of the experimental set-up turns out to be very small and indeed would be appropriate for micro flow investigations, this is not in the focus of our study. The motivation for a set-up according to Fig. 1 is to have an experimental device for general laminar flows. The particular dimensions are fixed by the size of commercially available silicon wafers which have a diameter of 100 mm.

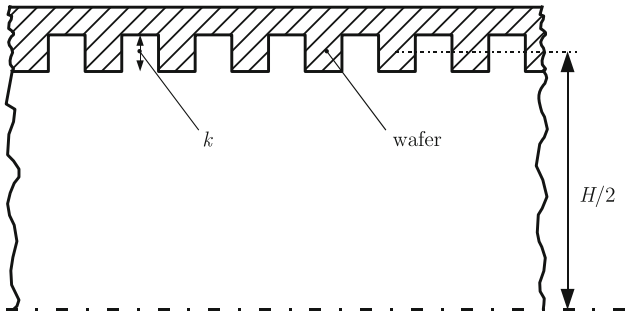

Fig. 2 Roughness parameter k for the rough channel of size H

2.2 Surface structuring technique

The surface roughness structures on the wafers are fabricated in a micro machining process (see Fig. 3). As substrate material a 525 µm thick and 100 mm in diameter silicon wafer is used. The wafer has a polished surface with a flatness (TTV - total thickness variation) lower than 3 µm and a surface roughness R_a better than 1 µm (step a). The wafer is spin-coated with a 17.5-µm-thick photo-resist layer. The surface structure is transferred to the resist using a chromium mask and an ultra-violet light source. After developing the resist, hence removing the exposed areas (step b), the silicon is etched in an inductively coupled plasma (ICP) advanced silicon dry etching process (step c). The etch rate is about 1.5 µm/min and increases slightly from the centre to the edge of the wafer. A targeted depth of 20 µm in the centre results in approximately 25 µm deep grooves at the edge. Finally, the photo-resist is removed leaving the wafer with the targeted roughness (step d), see also Fig. 4 for some details of the actual roughness shape.

Using this technique, four wafers with different kinds of regular roughness were produced. Roughness elements on the wafer surface are circular grooves with different depth and width, always one width apart from each other. Table 1 provides the geometrical details of all four wafers.

2.3 Details and data acquisition

Figure 5 gives more details of the experimental facility and the data acquisition in it. Note especially the measurement of the channel height (6), flow rate (7), temperature

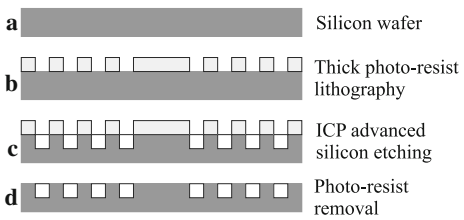

Fig. 3 Micro-machining fabrication steps *a–d* for the groove structures

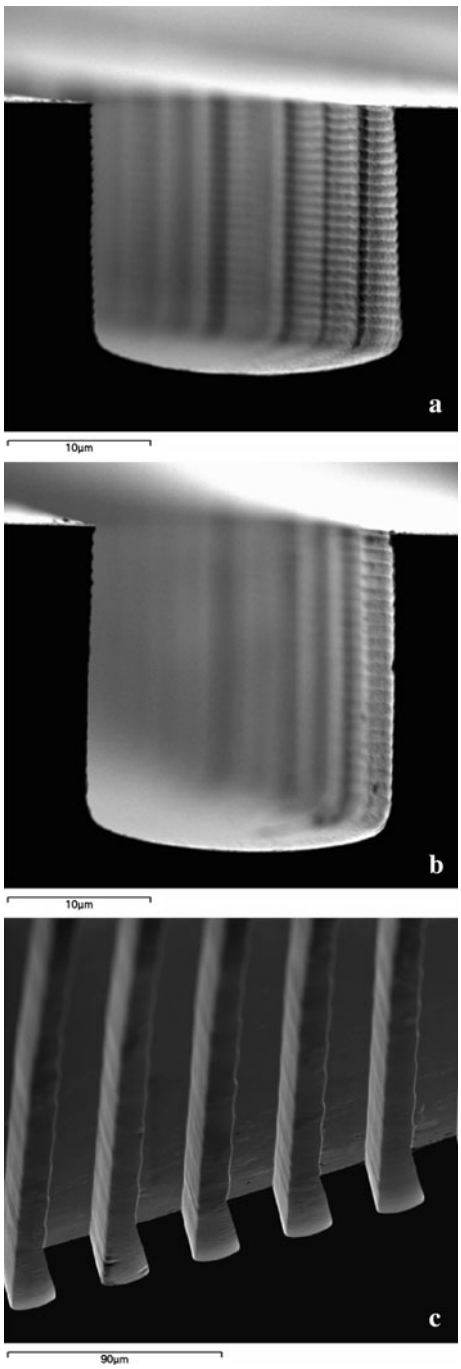

Fig. 4 Scanning electron microscope (*SEM*) pictures of the cross-section of a groove in the center (**a**) and at the edge (**b**) and multiple grooves (**c**) in the wafer. Note: in **c** the black part is scarp surface

(9, 10), and pressure (11, 12). Details with respect to the measurement of these four crucial quantities are

- channel height: Mahr®, Extramess 2000, 0–500, ±0.3 µm
- mass flow rate : Bronkhorst®, EL-FLOW F-111C, 0–0.3 and 0–6 l/min, ±0.1%

Table 1 Geometrical details of the surface roughness; grooves are at a radial distance between 10 and 50 mm

Wafer	Width (μm)	Depth (μm)	Number of grooves
I-2020	20	20	1,000
II-2030	20	30	1,000
III-3030	30	30	660
IV-3004	30	4	660

- temperature: I.E.D.®, Thermocouple THERM2-K8, 0–160°C, ±0.5 K
- pressure: Halstrup Walcher®, PU-2266 0–100 Pa, ±0.25%
  GE Druck Messtechnik GmbH, LPM 9481-82L, 0–10^5 Pa, ±0.1%

Alltogether 12 pressure holes are bored into the lower plate in order to measure the pressure distribution along the channel. Figure 6 shows their positions, spiraling around the center. By this arrangement, we avoid disturbances from upstream pressure holes and simultaneously can check the radial symmetry of the flow.

Figure 6 also shows the diameter of the pressure holes, to be 0.7 and 1.8 mm wide. This is quite large compared to the hydraulic diameters of the channels. However, detailed CFD simulations indicate that there is no influence of the size of the pressure holes on the measured pressure in the channel.

Figure 7 shows the central part of the experimental facility with an actual channel height set to 110 μm, indicated by the displays of all three distance meters.

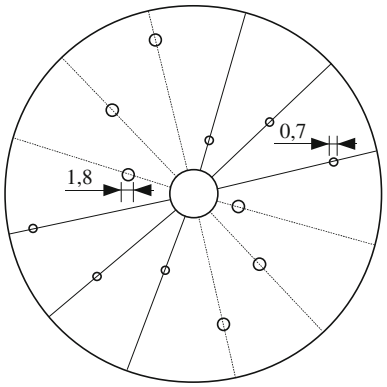

Fig. 6 Position of the pressure holes spiraling around the center; 6 small (0.7 mm) and 6 large (1.8 mm) holes

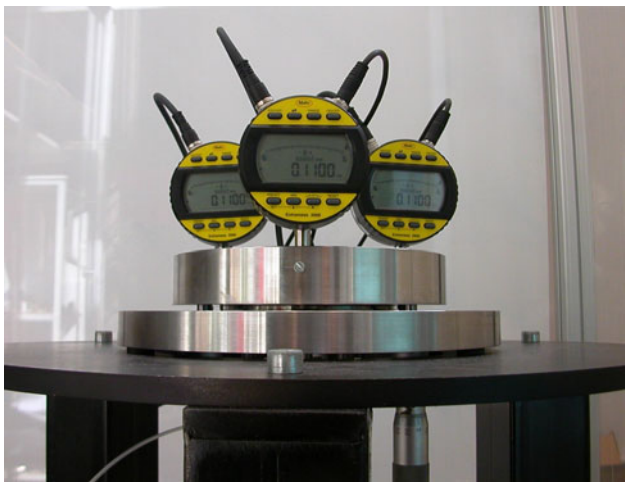

Fig. 7 Photography of the experimental facility

3 Data evaluation

A rough wall, compared to a smooth one, leads to a higher dissipation rate in the fluid and thus causes a higher loss in total head of a flow through a confined space like in pipes or channels.

Note that the commonly used term “pressure loss” is correct only when the flow is fully developed and

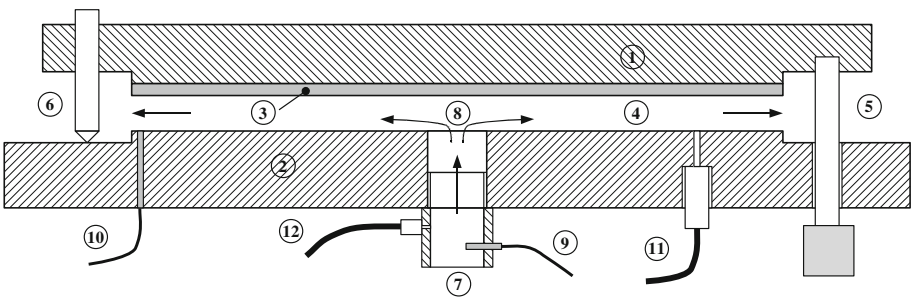

Fig. 5 Details of the experimental facility and data aquisition

horizontal, otherwise, part of the pressure change is not a "loss". From a thermodynamic point of view what is lost is *exergy*, i.e. that part of the energy that can be freely converted into any other form of energy. This is correctly accounted for by the term "loss of total head", i.e. loss of mechanical energy (which as a whole is exergy).

3.1 Pressure measurements

In our experimental set-up, we measure the radial pressure distribution, i.e. the pressure distribution in streamwise direction. Figure 8 shows a typical measurement in a smooth channel of width 400 µm.

The pressure drop in the radial (streamwise) direction is not only due to losses (of total head, i.e. exergy), but also due to the radial change of kinetic energy (which is no loss). This additional part could be subtracted from the measured p-distribution since it is known from theoretical considerations of the flow.

Since, however, we do not want to mix measured and calculated data at this stage, we still use the measured data, carefully keeping in mind their physical interpretation.

In Fig. 8, the solid line is an interpolation curve to the data in a smooth channel. Its general form is

$$p - p_e = \frac{27\,\dot{m}^2}{140\pi^2\varrho H^2}\left(\frac{1}{r_e^2} - \frac{1}{r^2}\right) + C\frac{6\,\mu\dot{m}}{\pi\varrho H^3}\ln\left(\frac{r_e}{r}\right) \qquad (1)$$

which can be derived as a series expansion in $1/r$ with a truncation error $(1/r)^4$, (cf. Savage 1964).

Here, $\dot{m}$ is the mass flux, ϱ the density, μ the viscosity, and p_e the pressure at the exit radius r_e. Equation 1 is based on the assumption of a locally fully developed channel flow leaving $C \neq 1$ as an interpolation parameter. The first term in (1) is the pressure change due to the redistribution of kinetic energy. The second term corresponds to the total head loss (cf. Gloss 2009).

Also shown in Fig. 8, as a dashed line, is the result of a numerical simulation of the flow which will be discussed later.

In order to quantify the influence of wall roughness, a ratio called "roughness influence number Λ" is introduced,

$$\Lambda_{meas} = \frac{(\Delta p_{meas})_{rough}}{(\Delta p_{meas})_{smooth}} \qquad (2)$$

Here, Δp is a typical pressure difference in our set-up, from now on set to $\Delta p = p_1 - p_e$ with p_e as the pressure at the exit and p_1 as the pressure at the first pressure hole at radius $r = 22$ mm.

For rough walls, we expect Λ to be above $\Lambda = 1$ with Λ further increasing for increasing values for the relative wall roughness $K = k/H$.

3.2 Error analysis

With four quantities to measure and the radial extent R of the flow field, the error in the final result, i.e. in Λ, can be determined as

$$\frac{\delta\Lambda}{|\Lambda|} = 3\frac{\delta H}{|H|} + 2\frac{\delta\Delta p}{|\Delta p|} + 2\frac{\delta T}{|T|} + 2\frac{\delta R}{|R|} + \frac{\delta\dot{m}}{|\dot{m}|} \qquad (3)$$

With the specific parameter values of our experiments (according to Table 2), typical deviations $\delta\Lambda/|\Lambda|$ are of the order of 1–5%. These numbers are shown as error bars in some of the diagrams below.

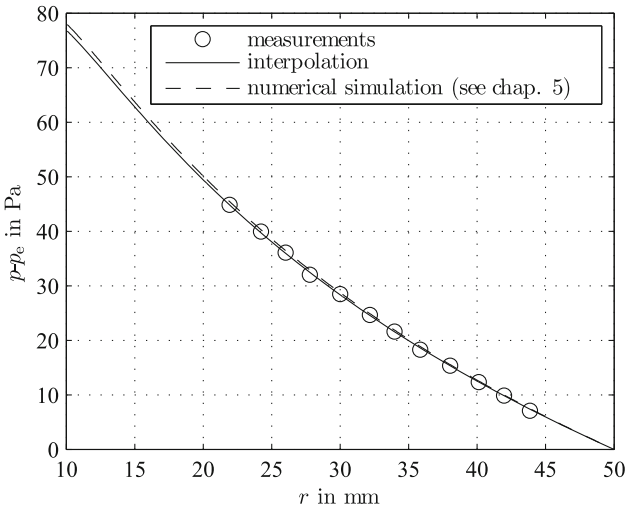

Fig. 8 Pressure distribution in a channel; r radial (streamwise) direction, p_e pressure at the exit

4 Measurements

The effect of wall roughness in terms of the ratio Λ_{meas} according to (2) was measured for all four wafers described in Table 1. Figure 9 shows that there is a clear trend for Λ to exceed $\Lambda = 1$ with increasing relative roughness K. The measurements were very time consuming so that Fig. 9

Table 2 Root mean square deviations of the sensors (%-data: percent of measurement range)

Sensor	Quantity	Meas. range	Accuracy
Distance meter	H	0–500 µm	0.3 µm
Mass flux sensor	$\dot{m}$	0–0.3 l/min	0.1%
		0–6 l/min	
Thermo couple	T	0–160°C	0.5 K
Pressure sensor	Δp	0–100 Pa	0.25%
		$0–10^5$ Pa	0.1%

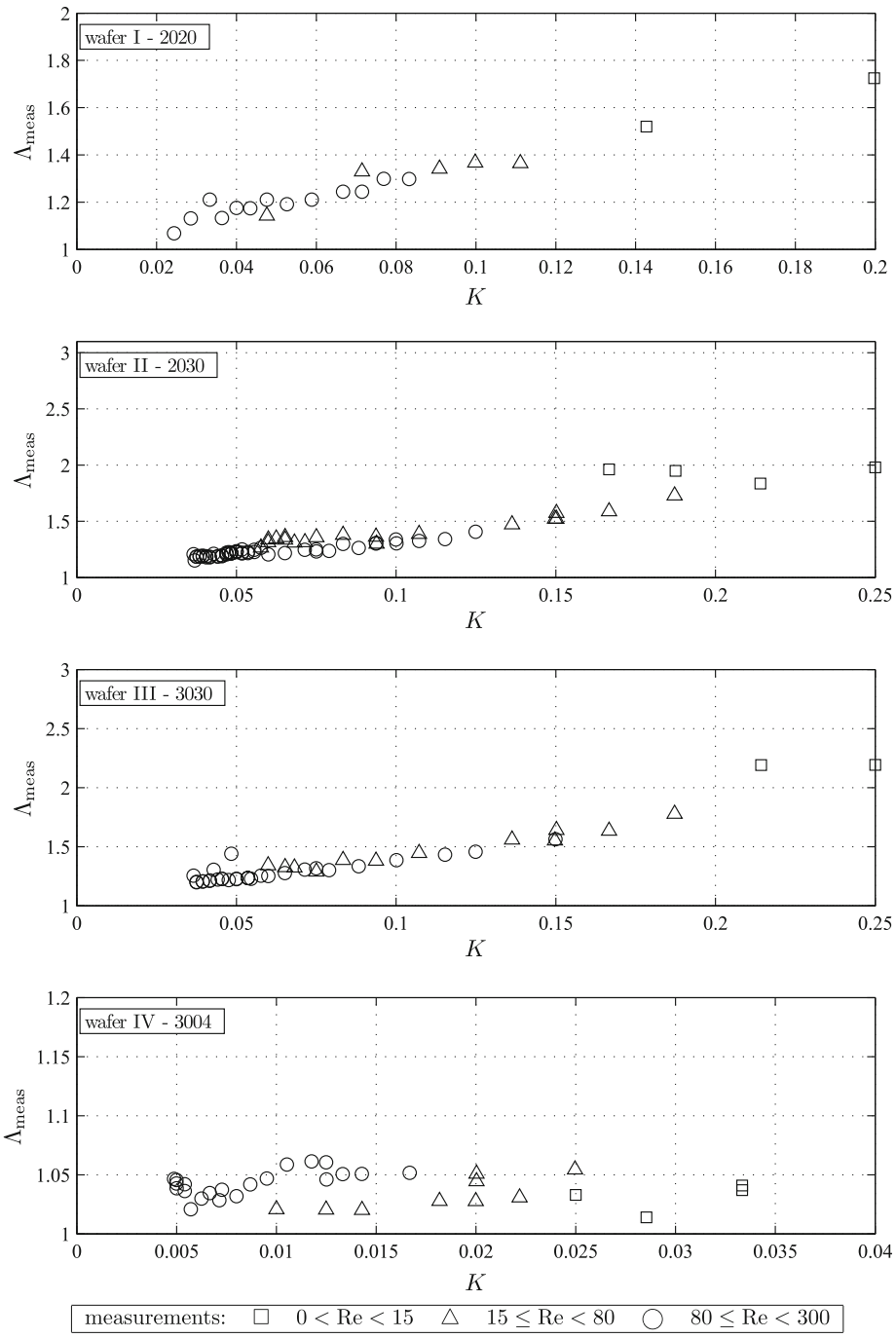

Fig. 9 Experimentally determined Λ_{meas}-ratios for all four wafers in Table 1

shows results that were gained in a period of about eight weeks.

For the sake of clarity, error bars are not included in Fig. 9. They are exemplified in Fig. 10 for the wafer I-2020.

For very small Reynolds numbers (i.e. for $Re \rightarrow 0$), the local flow around the roughness elements has the character of a creeping flow for which there are only pressure and friction forces. With only two forces in balance, there is no parameter in the problem.

For large Reynolds numbers, however, inertia forces come in and the balance of forces close to the roughness element is that of pressure, friction, and inertia forces. The balance of three forces is always characterized by a parameter which here is the Reynolds number. That is why there is a Reynolds number dependence in the results shown in Figs. 9 and 10, respectively.

Since we want to compare the measurements with theoretical results gained from numerical calculations, we have to account for that Reynolds number dependence. At

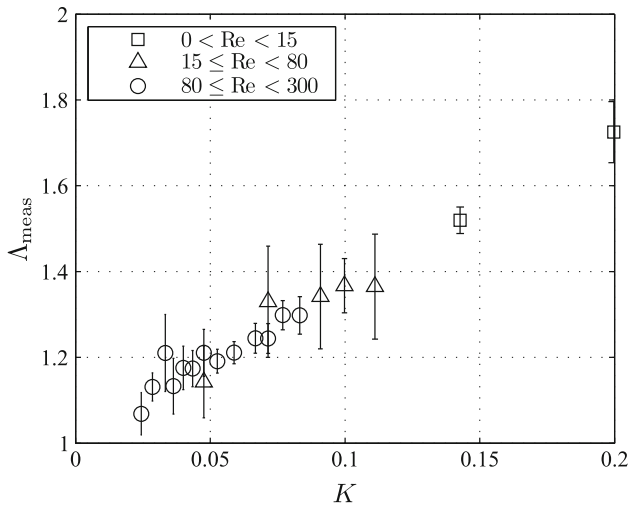

Fig. 10 Results for wafer I-2020, see Fig. 9, now with *error bars* included

least for the wafers I, II, and III, however, the Reynolds number dependence is rather weak. This is why we only group the measurements into three categories, i.e. with small (0–15), medium (15–80) and large (80–300) Reynolds numbers.

Only for wafer IV, there is a stronger Reynolds number dependence which can be explained as following. In general, there is a Reynolds number dependence of Λ (measured or simulated) whenever the Reynolds number dependence of the rough wall case is different from that of the smooth wall case, since Λ according to (2) and (8) below refers these two cases to each other. The kind of Reynolds number dependence basically depends on the strength of inertia forces. Without inertia forces $\Delta p \sim u_\mathrm{m}$ whereas a dominance of inertia forces results in $\Delta p \sim u_\mathrm{m}^2$.

Wafers I, II, and III have grooves with ratios $k/h \approx 1$, where h is the width of the grooves. In these almost square shaped cavities, one big vortex forms with an outer flow above it that does not exhibit strong local accelerations. Therefore, the overall inertia forces are similar to those of the smooth wall case.

Wafer IV, however, has a ratio $k/h = 0.133$. For the "outer" flow above these grooves, the wall shape now is one with backward and forward facing steps which locally lead to high accelerations and decelerations, i.e. appreciably higher local inertial forces than in the corresponding smooth wall case. As a consequence, the overall Reynolds number dependence of the rough wall case for wafer IV differs from that of the corresponding smooth wall case much stronger than this is the case for wafers I, II, and III, resulting in a stronger Reynolds number dependence of the wafer IV results for Λ.

In the turbulent case, wafers I, II, and III would be called to be of d-type, whereas wafer IV has a k-type roughness, see Perry et al. (1968). The physics of turbulent and laminar flows are so different, however, that the only common feature is a difference in impact of the two types of roughness in both cases, laminar and turbulent.

5 Numerical simulations

With the experimental results of our study, we want to validate a numerical model with which the influence of wall roughness can be determined by means of a numerical simulation.

Once such a model is validated, it can serve as a reliable alternative to the experimental determination of the roughness impact on laminar flows through conducts with various cross sections and roughness shapes.

To have such a model is desirable since neither the hydraulic diameter concept nor the sand roughness approach (cf. Nikuradse 1933) holds in the case of laminar flows. As a consequence, there has to be a case by case determination of the roughness impact.

5.1 The dissipation model

A loss of total head, i.e. mechanical energy and thus exergy, respectively, correspond to the production of entropy in a dissipation process. If this entropy production can be determined in detail, i.e. locally in a flow field, an integration of this field quantity will immediately provide the loss in terms of a loss coefficient. Calculating the local entropy production due to dissipation in a laminar flow field is straightforward. Basically, only the local specific entropy production rate

$$\dot{S}_\mathrm{D}''' = \frac{\mu}{T}\left(2\left[\left(\frac{\partial u}{\partial x}\right)^2+\left(\frac{\partial v}{\partial y}\right)^2+\left(\frac{\partial w}{\partial z}\right)^2\right]+\left(\frac{\partial u}{\partial y}+\frac{\partial v}{\partial x}\right)^2 + \left(\frac{\partial u}{\partial z}+\frac{\partial w}{\partial x}\right)^2+\left(\frac{\partial v}{\partial z}+\frac{\partial w}{\partial y}\right)^2\right) \tag{4}$$

has to be determined, see Herwig et al. (2008b) for details. From this field quantity, a friction factor $f \equiv (\mathrm{d}\varphi/\mathrm{d}x)4H/u_\mathrm{m}^2$ can be determined by integrating $\dot{S}_\mathrm{D}'''$ over a cross section of the flow field including all spaces between the roughness elements. Here, $\mathrm{d}\varphi/\mathrm{d}x$ is the specific dissipation rate per length. Its relation to the entropy production is by

$$\frac{\mathrm{d}\varphi}{\mathrm{d}x} = \frac{T\dot{S}_\mathrm{D}'}{\dot{m}} \tag{5}$$

with $\dot{S}_\mathrm{D}'$ as entropy production rate in a cross section, T the temperature in Kelvin, and $\dot{m}$ the mass flux. However, at a specific location x, the cross section including the spaces

between the roughness elements (slightly) varies depending on the exact location with respect to the roughness element (peak or trough). Therefore, instead of $\mathrm{d}\varphi/\mathrm{d}x$ finite values, $\Delta\varphi/\Delta x$ should be determined with $\Delta x \gg k$ and $\Delta x < H$.

Then

$$\Delta\varphi = \frac{T\dot{S}'_{\mathrm{D}}\Delta x}{\dot{m}} = \frac{T\dot{S}_{\mathrm{D}}|_{\Delta x}}{\dot{m}} \tag{6}$$

with $\dot{S}_{\mathrm{D}}|_{\Delta x}$ as entropy production rate in the volume of extend Δx.

In channels with constant cross sections, Δx can be extended to a finite length L_{12} between two cross sections 1 and 2 with the specific energy dissipation rate φ_{12} between them and

$$\varphi_{12} = \frac{T\dot{S}_{\mathrm{D}}|_{12}}{\dot{m}}. \tag{7}$$

Equation (7) is appropriate to determine a friction factor $f_{12} \equiv (\varphi_{12}/L_{12})4H/u_{\mathrm{m}}^2$ for fully developed flows in various geometries.

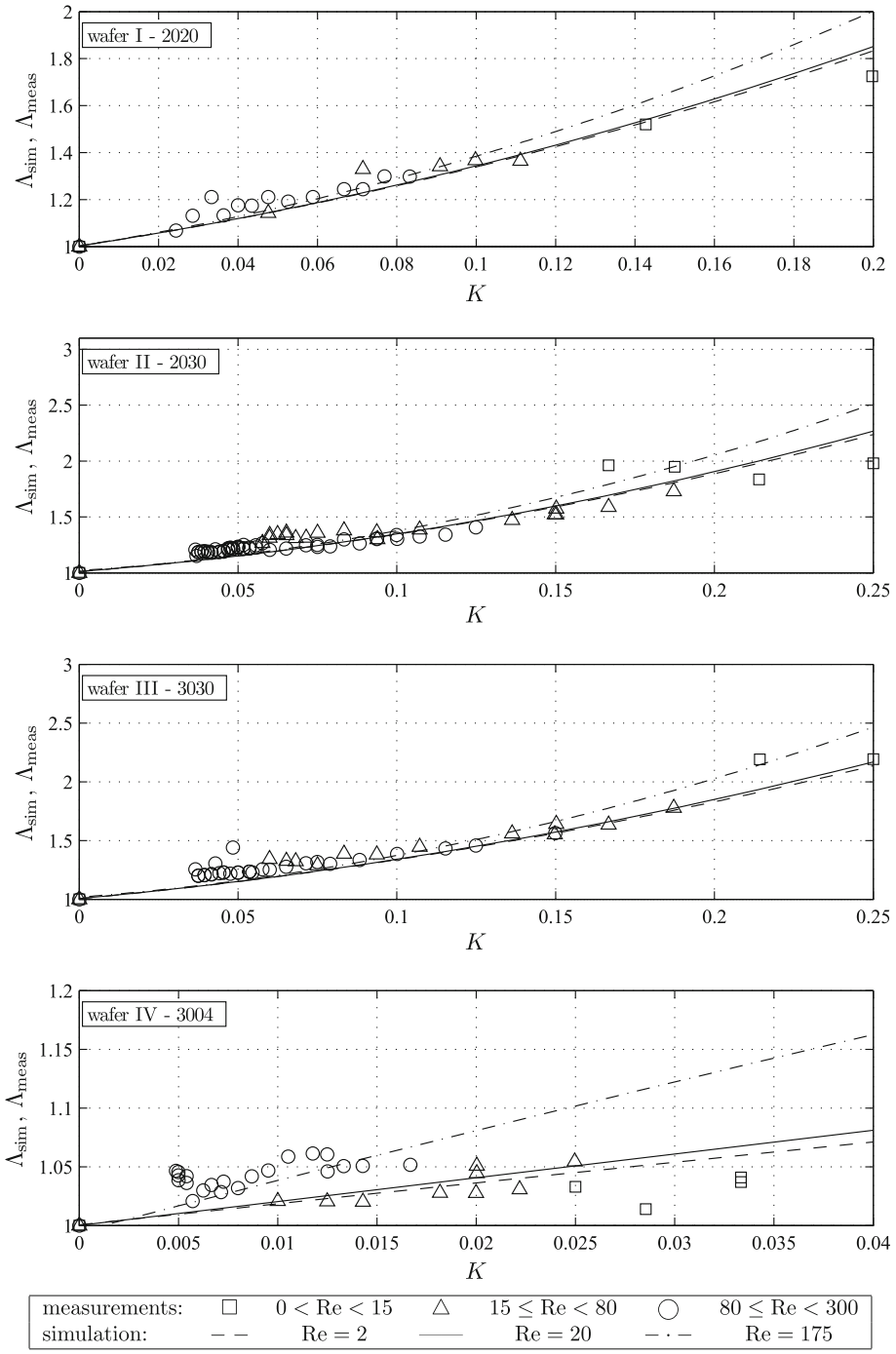

Fig. 11 Experimental (Λ_{meas}) versus numerical (Λ_{sim}) results for the four wafers in Table 1

5.2 Validation of the dissipation model

Using the CFD package FLUENT® 6.3, the dissipation model was applied to a computational geometry matching that of our experimental set-up exactly (including the four different wafers I–IV).

The computations were performed in a two-dimensional axi-symetric domain. A second order upwind scheme with a specified mass flow boundary condition at the inlet was used. Up to 5 million nodes were used in a hybrid structured–unstructured grid ensuring grid independence for the solution, with a finer resolution close to the rough wall. Convergence was met when the maximum normalized residual fell below 10^{-10}. Typical computational times on the Xeon 2.0 GHz DualCore processors exceeded 12 h, see Gloss (2009).

The grid independent results of these numerical simulations are compared to the experimental results (see Fig. 9) in Fig. 11.

Three different Reynolds numbers were chosen ($Re = 2$, 20 and 175) in order to show the behaviour of

$$\Lambda_{\mathrm{sim}} = \frac{(\Delta p_{\mathrm{sim}})_{\mathrm{rough}}}{(\Delta p_{\mathrm{sim}})_{\mathrm{smooth}}} \tag{8}$$

with increasing Reynolds numbers. Here, Λ_{sim} is introduced as a ratio Λ for simulation results analogous to Λ_{meas} in (2). It can be evaluated once Δp has been determined from the numerical solutions for the dissipation process.

We judge the agreement of the experimental and numerical results in Fig. 11 as a validation of the numerical dissipation model, especially on the background of the moderate accuracy of the experiments shown by the error bars in Fig. 10. With this moderate accuracy, we refrain from making a detailed analysis of the Reynolds number dependence. Instead, we state that the trend of Λ increasing for increasing Reynolds numbers is the same for the experiments (with the categories of small, medium, and large Re) and the simulations (with distinct Reynolds numbers 2, 20, and 175).

6 Conclusions

With the experiments shown, we could demonstrate that there is a non-negligible influence of wall roughness for laminar flows. We also use our experimental data for the validation of a numerical model based on entropy production considerations.

With this model, we now can determine the influence of wall roughness in any geometry and for arbitrary kinds of wall roughness.

As an example, Fig. 12 shows the famous Moody chart here specified for a pipe geometry with groove wall roughness like that of wafer I in Table 1, see also Fig. 2. The lines for $K = 0.05$ and $K = 0.1$ show that the influence of wall roughness is stronger in turbulent flows but not negligible in laminar flows.

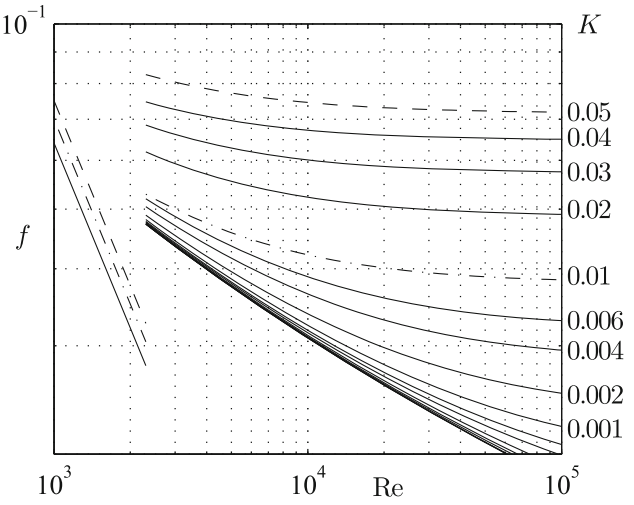

Fig. 12 Moody chart for a pipe with groove wall roughness; $K = 0.05$: *dashedline* & $K = 0.01$: *dotdashedline* (see Table 1, wafer I for the roughness geometry)

For laminar flows, the hydraulic diameter concept cannot be applied nor does the sand roughness equivalence hold.

Thus, different from the turbulent case, for laminar flows, the geometry as well as the kind of wall roughness has to be specified when also the laminar part in a friction chart $f = f(K, Re)$ should be correct.

Acknowledgments The authors want to thank Dr. Sid Becker/North Carolina State University and Humboldt Fellow at TU Hamburg-Harburg for his assistance in preparing the final version of this paper.

References

Brackbill TP, Kandlikar SG (2007) Effects of low uniform relative roughness on single-phase friction factors in microchannels and minichannels. In: Proceedings of the fifth international conference on nanochannels, microchannels and minichannels

Croce G, D'Agaro P (2005) Numerical simulation of roughness effects on microchannel heat transfers and pressure drop in laminar flow. J Phys D Appl Phys (38):1518–1530

Gloss D (2009) Der Einfluss von Wandrauheiten auf laminare Strömungen: Untersuchungen in Mikrokanälen. Cuvillier Verlag, Göttingen. ISBN 978-3-86727-962-8. PhD thesis

Hao P-F, Yao Z-H, He F, Zhu K-Q (2006) Experimental investigation of water flow on smooth and rough silicon microchannels. J Micromech Microeng 16:1397–1402

Herwig H (2002) Flow and heat transfer in micro systems: is everything different or just smaller? ZAMM-Z Angew Math Mech 82(9):579–586

Herwig H, Gloss D, Wenterodt T (2008a) Flow in channels with rough walls—old and new concepts. In: Proceedings of the sixth international conference on nanochannels, microchannels and minichannels, ICNMM2008-26064

Herwig H, Gloss D, Wenterodt T (2008b) A new approach to understand and model the influence of wall roughness on friction factors for pipe and channel flows. J Fluid Mech (613):35–53

Hu Y, Werner C, Li D (2003) Influence of three-dimensional roughness on pressure-driven flow through microchannels. J Fluid Eng (125):871–879

Ji Y, Yuan K, Chung JN (2005) Numerical simulation of wall roughness on gaseous flow and heat transfer in a microchannel. Int J Heat Mass Transf 49:1329–1339

Kandlikar SG (2005) Roughness effects at microscale—reassessing nikuradse's experiments on liquid flow in rough tubes. Bull Acad Sci 53

Kleinstreuer C, Koo J (2004) Computational analysis of wall roughness effects for liquid flow in micro-conduits. J Fluids Eng 126:1–9

Lilly TC, Duncan JA, Nothnagel SL, Gimelshein SF, Gimelshein NE, Ketsdever AD, Wysong IJ (2007) Numerical and experimental investigation of microchannel flows with rough surfaces. Phys Fluids 19:106101 1–9

Munson BR, Young DF, Okiishi TH (2005) Fundamentals of fluid mechanics, 5th edn. John Wiley & Sons Inc., New York

Nikuradse J (1933) Strömungsgesetze in rauhen rohren. In: Forschung auf dem Gebiet des Ingenieurwesens, number 361 in VDI-Forschungsheft, pages 1–22. VDI-Verlag, Düsseldorf

Perry AE, Schofield WH, Joubert PN (1968) Rough wall turbulent boundary layers. J Fluid Mech 37:383–413

Rawool AS, Mitra SK, Kandlikar SG (2006) Numerical simulation of flow through microchannels with designed roughness. Microfluid Nanofluid 2:215–221

Savage SB (1964) Laminar radial flow between parallel plates. J Appl Mech 31:594–596

Schlichting H, Gersten K (2006) Grenzschicht-Theorie, 10th edn. Springer, Berlin

White FM (2008) Fluid mechanics, 6th edn. McGraw-Hill, New York

Wu PY, Little WA (1983) Measurement of friction factors for the flow of gases in very fine channels used for microminiature joule-thomson refrigerators. Cryogenics 23(5):273–277

Zierep J (2008) Grundzüge der Strömungslehre, 7th edn. Vieweg Verlag, Wiesbaden